Lithium Ion Induced Nanophase Ordering and Ion Mobility in Ionic Block Copolymers

Eirini F. Ioannou, Grigoris Mountrichas, Stergios Pispas, and Efstratios I. Kamitsos*

Theoretical and Physical Chemistry Institute, National Hellenic Research Foundation, 48 Vass. Constantinou Ave., 116 35, Athens, Greece

George Floudas*

Department of Physics, University of Ioannina, P.O. Box 1186, 451 10, Ioannina, Greece, and Foundation for Research and Technology−Hellas, Biomedical Research Institute (FORTH-BRI)

Received April 17, 2008; Revised Manuscript Received June 13, 2008

ABSTRACT: Diblock copolymers of poly(styrene-*b*-methacrylic acid) (PS−PMAA) of various compositions have been synthesized by anionic polymerization and were employed as templates for the development of "single-ion" polymer electrolyte systems. Lithium ions were introduced as the effective component that alters the phase state and contributes to ionic conductivity of these block polyelectrolytes. The local structure, microdomain morphology, and ion dynamics of the pure block copolymers and of the block polyelectrolytes were investigated by infrared spectroscopy, small-angle X-ray scattering, differential scanning calorimetry, and dielectric spectroscopy. Investigation of the microdomain structure revealed complexation of lithium ions with the carboxylate units of the PMAA phase in two types of coordination (chelating vs bringing) that alters the phase state of the copolymers and results in a change from the weak- to strong-segregation limit. The investigation of dynamics revealed a new dielectrically active process associated with a local relaxation of lithium ions coupled to the MAA segments via the two types of coordination. The ionic conductivity of the block polyelectrolytes was found enhanced by about 3 orders of magnitude relative to that of the parent copolymers. These results contribute to a better understanding of the changes in microdomain morphology as well as of the ion dynamics in systems resulting from the association of lithium ions with the charged PMAA block.

1. Introduction

In recent years interest has been focused on solid-state materials that exhibit enhanced ion transport properties. Among them, polymer solid electrolytes constitute a class of materials of high promise for technological applications including batteries, fuel cells, and other electrochemical devices.[1,2] The advantages of using polymer solid electrolytes include lack of corrosive liquids, wide potential electrochemical stability, improved mechanical properties, and ability for thin film processing.[3,4]

To satisfy such performance requirements, research efforts have been focused on the design of solid electrolytes from block copolymers,[5,6] which are materials that consist of two chemically dissimilar polymers bonded covalently end-to-end. Under appropriate conditions and compositions they self-organize into various nanostructures as a result of microphase separation between incompatible blocks.[7] When a lithium-salt-solvating polymer is chosen as one of the block components, continuous, nanoscopic ion-conducting pathways can form.[8] One suitable polymer with ionic groups forming complexes with metal ions is poly(methacrylic acid) (PMAA), the complexation ability of which has been investigated under different experimental conditions, i.e., as a homopolymer[9] or as a component in ionomers.[10,11]

In the present study, diblock copolymers of poly(styrene-*b*-methacrylic acid) (PS−PMAA) of various compositions have been prepared by anionic polymerization and were employed as templates for the development of polymer electrolyte systems. Lithium ions were introduced as the effective component that alters the phase state and contributes to ionic conductivity of these block polyelectrolytes. The aim of this work is (i) to investigate the effect of ion substitution on the block copolymer phase state and (ii) to understand ion dynamics in systems resulting from the association of lithium ions with the PMAA charged block. The latter is of significant importance for understanding the bulk physicochemical behavior of the final ionic block polyelectrolytes. The thermodynamics of the synthesized block polyelectrolytes were investigated by differential scanning calorimetry (DSC) and their supramolecular self-assembly by small-angle X-ray scattering (SAXS). Structural aspects at the atomic/molecular level were explored by infrared spectroscopy (IR), while polymer and ion dynamics were studied by dielectric spectroscopy (DS).

2. Experimental Section

2.1. Materials. *Synthesis of the Precursor Block Copolymers.* A number of poly(styrene-*b*-*tert*-butyl methacrylate) (PS−P*t*BMA) block copolymers, with different ratios of each block and overall molecular weights, were synthesized by anionic polymerization high-vacuum techniques.[12] Purification of all reagents (solvents, monomers, etc.) was accomplished according to well-established procedures. The block copolymers were prepared by polymerizing first the styrene, using *n*-butyllithium as initiator in benzene, followed by the addition of *tert*-butyl methacrylate to the living polystyryllithium to give the second block. Polymerizations took place in THF at −78 °C. Initially, the addition of *n*-BuLi as a solution in hexane was carried out followed by the distillation of styrene. The polymerization of the first block was carried out for 1 h followed by the addition of diphenylethylene (DPE:Li = 2:1) and LiCl (LiCl:Li = 5:1) in order to reduce the reactivity of the living polystyryllithium chain ends. Subsequently, the addition of the second monomer, *tert*-butyl methacrylate, was also carried out by distillation into the polymerization reactor. The polymerization of the second monomer was continued for 30 min after distillation was completed. The polymerization reaction was then terminated by the addition of degassed methanol to give the desired precursor

* To whom correspondence should be addressed.

10.1021/ma8008542 CCC: $40.75
Published on Web 07/23/2008

Scheme 1. Reaction Scheme Leading to the Synthesis of the Diblock Copolymers and the Resulting Block Polyelectrolytes

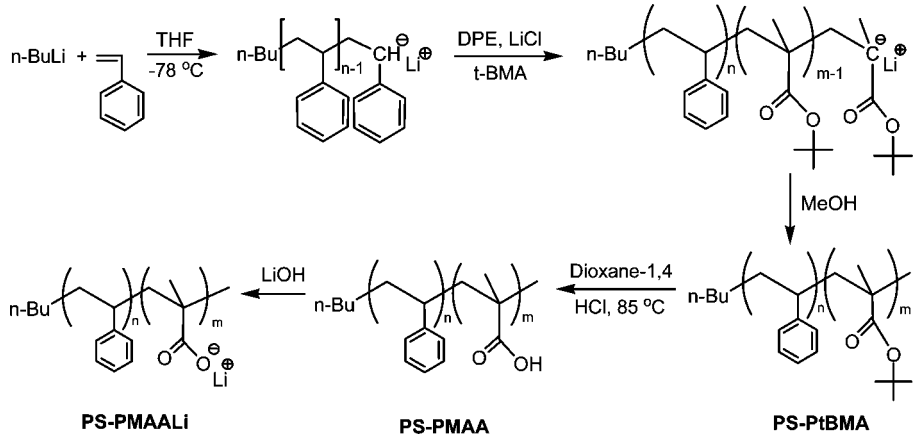

block copolymers (PS−P*t*BMA), which were subsequently isolated by precipitation in methanol/water mixture and dried under vacuum before further use.[13]

The molecular weight and molecular weight distribution data for the precursor polymers were obtained by size exclusion chromatography, using a Waters system composed of a Waters 1515 isocratic pump, a set of three μ-Styragel mixed bed columns, with a porosity range of 10^2-10^6 Å, and a Waters 2414 refractive index detector. The entire system was calibrated by polystyrene standards (M_w: 2500−900 000) and was controlled through Breeze software. Tetrahydrofuran was used as the mobile phase at a flow rate of 1.0 mL/min at 40 °C. Composition of the copolymers was determined by ^{1}H NMR spectroscopy in $CDCl_3$ at 30 °C, using a Bruker AC 300 instrument.

Hydrolysis of PtBMA Block. The synthesis of the corresponding poly(styrene-*b*-methacrylic acid) (PS−PMAA) block copolymer requires the hydrolysis of the P*t*BMA block. For a typical hydrolysis reaction, the desired amount of the diblock (PS−P*t*BMA) was dissolved in dioxane-1,4 in a 50 mL round-bottom flask at 5 wt % concentration.[13] A 5-fold molar excess of concentrated HCl, with respect to the ester groups, was added, and the temperature was raised to 85 °C. The solution was refluxed for 6 h, and after the end of the reaction it was cooled to room temperature. The product (PS−PMAA) was dried to a constant weight under vacuum.

Neutralization with LiOH. At first 5% (w/v) solutions of the PS−PMAA diblock copolymers were prepared in a mixture of tetrahydrofuran and methanol. Weighted amounts of LiOH for 100% neutralization of the hydroxyl groups of the PMAA block were also prepared in 5% (w/v) water solutions. Each LiOH solution was added dropwise to its corresponding diblock copolymer's solution, and the final products were isolated by evaporation of the solvents and dried to a constant weight under vacuum. The reaction route leading to the synthesis of the diblock copolymers and the resulting block polyelectrolytes is presented in Scheme 1. The molecular characteristics of the initial diblock copolymers and of the resulted block polyelectrolytes are summarized in Table 1. It is noted that the volume fractions were calculated as

$$f_{\mathrm{PMAA,Li}} = \left[1 + \left(\frac{1}{w_{\mathrm{PMAA,Li}}} - 1\right)\frac{\rho_{\mathrm{PMAA,Li}}}{\rho_{\mathrm{PS}}}\right]^{-1} \quad (1)$$

where $\rho_{\mathrm{PS}} = 1.05$ g/cm^3 [14] and $\rho_{\mathrm{PMAA}} \approx \rho_{\mathrm{PMAALi}} = 1.36$ g/cm^3.[14]

2.2. Characterization Methods. *Differential Scanning Calorimetry (DSC).* A Mettler Toledo Star differential scanning calorimeter (DSC), with capabilities of programmed cyclic temperature runs over the range of 113−673 K, was used for thermal analysis. The samples were first heated at a rate of 10 K/min from ambient temperature to 433 K and then cooled to 173 K at 10 K/min. A second heating run was conducted with the same rate, and it was used to identify the "low" glass transition temperature associated with the PS segments, T_g^{PS}, the width of the "transition", ΔT_g, and the change of the specific heat capacity, Δc_p, at T_g.

Table 1. Molecular Characteristics Including Molecular Weight, Distribution of Molecular Weights, Degrees of Polymerization, Composition by Weight and Volume Fraction of Methacrylic and Methacrylic-Salt Block in Diblock Copolymers and Block Polyelectrolytes, Respectively

sample	M_w[a]	M_w/M_n[b]	n/m[b]	$w_{\mathrm{PMAA,Li}}$ (wt %)[b]	$f_{\mathrm{PMAA,Li}}$[c]
SMAA1	44 900	1.06	363/83	16	0.13
SMAA1Li	45 500	1.06	363/83	18	0.14
SMAA2	34 500	1.06	239/112	28	0.23
SMAA2Li	35 400	1.06	239/112	30	0.25
SMAA3	29 200	1.06	160/146	43	0.35
SMAA3Li	30 300	1.06	160/146	45	0.37

[a] Calculated for the final copolymer, based on quantitative hydrolysis degree for block polyelectrolytes. [b] Values for the precursor block copolymers. [c] Based on 100% neutralization with LiOH for block polyelectrolytes.

Small-Angle X-ray Scattering (SAXS). An 18 kW rotating anode X-ray source (Rigaku) was used with a pinhole collimation and a two-dimensional (2D) detector (Bruker) with 1024 × 1024 pixels. A double graphite monochromator for the Cu Kα radiation (wavelength $\lambda = 0.154$ nm) was used, and the sample-to-detector distance was set at 1.8 m. The recorded 2D scattered intensity distributions were investigated over the azimuthal angle and are presented as a function of the scattering wave vector q ($q = (4\pi/\lambda)\sin(2\theta/2)$, where 2θ is the scattering angle). X-ray measurements were made on heating at 303, 333, 393, and 433 K and at the same temperatures on cooling, noting that 1 h long measurements were taken at each temperature with stability better than ±0.2 K. Identical SAXS images were obtained at the same temperature by heating and cooling. Since measurements at the two highest temperatures (i.e., 393 and 433 K) are above the glass temperature of the majority phase (PS), this suggests that these are likely the equilibrium microdomain morphologies. On the other hand, reaching complete equilibrium by exceeding the glass temperature of the PMAA phase requires high temperatures that could lead to sample decomposition.

FTIR Spectroscopy. Spectra in the mid-infrared region were measured on a Fourier transform spectrometer (Equinox 55, Bruker Optics) equipped with a single reflection diamond attenuated total reflectance (ATR) accessory (DuraSamplIR II, SENSIR). The spectra were measured over the 525−5000 cm^{-1} range at a resolution of 2 cm^{-1} and represent averages of 100 scans. ATR spectra were measured directly on sample powders, which were brought in contact with the diamond element using a torque press accessory.

Samples for far-infrared measurements were prepared by dispersing the polymer powders in low-density polyethylene and melting the mixture between two glass plates at ca. 100 °C to obtain ~0.5 mm thick films containing about 5 wt % block copolymer. Spectra in the far-infrared range (30−700 cm^{-1}) were measured in

transmission on a Fourier transform vacuum spectrometer (Vertex 80v, Bruker Optics). Each spectrum represents the average of 100 scans collected at 4 cm^{-1} resolution.

Dielectric Spectroscopy (DS). The sample capacitor for dielectric measurements consisted of two electrodes 20 mm in diameter, while the sample thickness was in the range of 50−80 μm. Dielectric measurements were performed at atmospheric pressure in the temperature range 173−523 K and in the frequency range 1×10^{-2}−1×10^{6} Hz, using a Novocontrol BDS system composed of a frequency response analyzer (Solartron Schlumberger FRA 1260) and a broadband dielectric converter. The complex dielectric permittivity $\varepsilon^* = \varepsilon' - i\varepsilon''$, where ε' is the real and ε'' the imaginary part, is a function of frequency, ω, temperature, T, and pressure, P, $\varepsilon^* = \varepsilon^*(\omega,T,P)$,[15] although here only the frequency and temperature dependences have been investigated.

For the analysis of DS spectra, the Havriliak−Negami (HN) equation[16] was employed:

$$\frac{\varepsilon^*(T,P,\omega) - \varepsilon_\infty(T,P)}{\Delta\varepsilon(T,P)} = \frac{1}{[1 + (i\omega\tau_{HN}(T,P))^m]^n} \quad (2)$$

where $\tau_{HN}(T,P)$ is the characteristic relaxation time, $\Delta\varepsilon(T,P) = \varepsilon_o(T,P) - \varepsilon_\infty(T,P)$ is the relaxation strength of the process under investigation, and m and n (with limits $0 < m$, $mn \leq 1$) describe the symmetrical and asymmetrical broadening of the distribution of relaxation times, respectively. The ε'' data were fitted at every temperature, while in some cases ε' data were also used as a consistency check. The linear rise of ε'' observed at low frequencies is due to the conductivity contribution, $\varepsilon'' \approx (\sigma_{dc}/\varepsilon_f)\omega^{-1}$, where σ_{dc} is the dc conductivity and ε_f is the permittivity of free space, and this has been included in the fitting procedure. From τ_{HN}, the relaxation time at maximum loss, τ_{max}, is obtained analytically from the following equation:

$$\tau_{max} = \tau_{HN}\left[\frac{\sin\left(\frac{\pi m}{2+2n}\right)}{\sin\left(\frac{\pi mn}{2+2n}\right)}\right]^{-1/m} \quad (3)$$

In a second approach, the electric modulus (M^*) and the conductivity (σ^*) representations were used, these quantities being interrelated with the dielectric permittivity through eqs 4 and 5:[17]

$$M^* = \frac{1}{\varepsilon^*} = M' + iM'' \quad (4)$$

$$\sigma^* = i\omega\varepsilon_0\varepsilon^* = \sigma' + i\sigma'' \quad (5)$$

The electric modulus representation is very sensitive to the process due to ionic mobility. The latter can be obtained from the frequency corresponding to crossing of the M' and M'' curves. The relaxation times corresponding to maximum ε'' and M'' are related through $\tau_{M''} = \tau_{\varepsilon''}(1 + \Delta\varepsilon/\varepsilon_\infty)^{-1/m}$ in the case of symmetric distribution ($n = 1$).[18]

3. Results and Discussion

3.1. Local Structure. Structural aspects at the molecular level were studied by infrared spectroscopy. Infrared spectra of a typical diblock copolymer acid (SMAA2) and of the block polyelectrolytes prepared by neutralizing the acids are shown in Figure 1, in a spectral region which is informative of the induced chemical changes. In order to facilitate comparison, the 698 cm^{-1} band was used for scaling the spectra since this reflects the out-of-plane skeleton bend vibration of the benzene ring of the PS block,[19,20] and thus, this band should be relatively unaffected by introducing Li^+ ions within the PMAA phase. Similarly, the band at 755 cm^{-1}, due to CH out-of-plane bend vibration of the benzene ring, would be independent of the presence of Li^+ ions. On the other hand, replacement of H^+ in the COOH group by Li^+ would affect mainly the vibrations of the carboxylic group because oxygen atoms of this group will

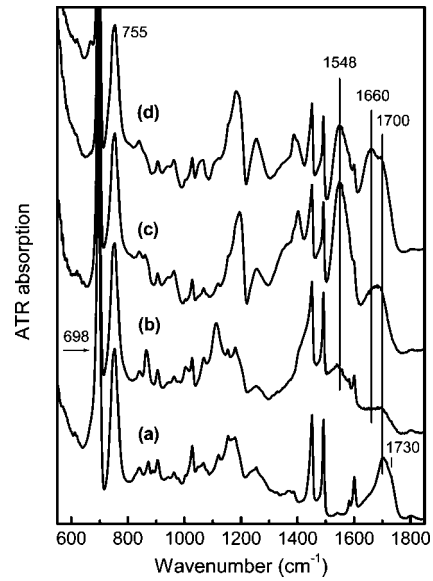

Figure 1. ATR absorption spectra of the diblock copolymer SMAA2 (a) and of the block polyelectrolytes resulted from the introduction of Li^+ ions in the PMAA phase: SMAA1Li (b), SMAA2Li (c), and SMAA3Li (d). The spectra are scaled on the 698 cm^{-1} band and offset to facilitate comparison.

form the coordination environment of Li^+ cations. Therefore, probing the vibrations of the carboxylic group would shed light on the structural evolution in the ionic domains of the block copolymer.

Hydrolysis of the PtBMA block results in the formation of PS−PMAA. The spectrum of the diblock copolymer acid SMAA2 (Figure 1) suggests that hydrolysis must be nearly quantitative,[13a] as indicated by the absence of a strong doublet at 1365, 1391 cm^{-1} due to characteristic bending vibration, $\delta_s(C(CH_3)_3)$, of the *tert*-butyl group.[20] Weak absorption at ca. 1368 and 1386 cm^{-1} arises from the bending vibration $\delta_s(CH_3)$ of the methyl groups.[20]

The infrared region 1300−1800 cm^{-1} provides information about local bonding in the PMAA phase because characteristic stretching vibrations of the carboxylic group and of the carboxylate anion are active in this region.[9,21–24] In particular, the band at 1700 cm^{-1} (Figure 1, SMAA2) can be attributed to the carbonyl stretching, ν(C═O), when the carboxylic acid forms hydrogen-bonded dimers, while the shoulder at ca. 1730 cm^{-1} can be associated with the corresponding mode of free acid groups.[21,23] As observed in Figure 1, absorption in the carbonyl region changes progressively as Li^+ ions are introduced in the ionic domains upon increasing the relative content of the PMAA−Li block. Most pronounced is the decrease of the relative intensity at ca. 1700 cm^{-1} while new bands develop at ca. 1660 and 1548 cm^{-1} as the Li−carboxylate content increases. On the basis of previous infrared studies of carboxylate salts including anhydrous lithium acetate,[9,21–24] the two new bands at 1660 and 1548 cm^{-1} can be taken to indicate the presence of carboxylate anions in two different coordination states with lithium ions. This is because the asymmetric stretching vibration of the carboxylate anion, $\nu_{as}(CO_2^-)$, is expected to give a strong infrared band in this frequency region. Thus, infrared intensity remaining at ca. 1700 cm^{-1} in the spectra of Li−carboxylate polyelectrolytes indicates a partial dissociation of the carboxylic acid.

The $\nu_{as}(CO_2^-)$ frequency can provide information on the carboxylate coordination geometry with metal ions, and two of the bonding modes of COO^- with Li^+ are of particular importance here: the chelating bidentate and the bridging bidentate.[9] In the chelating coordination, both oxygen atoms of

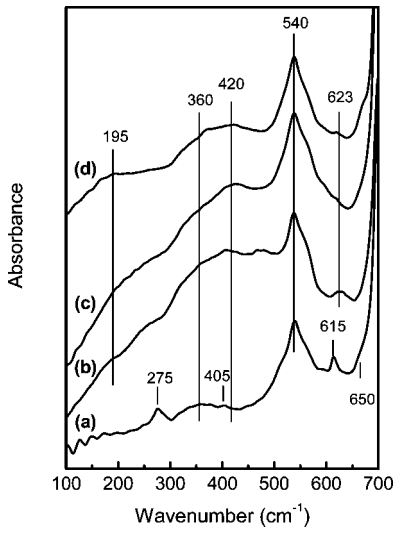

Figure 2. Far-infrared absorbance spectra of thin films of the diblock copolymer SMAA2 (a) and of the block polyelectrolytes in polyethylene: SMAA1Li (b), SMAA2Li (c), and SMAA3Li (d). The spectra are scaled on the 540 cm^{-1} band and offset to facilitate comparison.

one carboxylate unit are bonded to the same Li^+ ion, whereas in the bridging coordination the oxygen atoms of two COO^- anions are bonded to two different Li^+ ions forming a dimer-type arrangement, $2COO^-...2Li^+$. The presence of chelating coordination in the polyelectrolytes of this study is associated with the band at 1548 cm^{-1}, while the higher frequency band at 1660 cm^{-1} is consistent with bridging coordination.[9] For anhydrous lithium acetate two $\nu_{as}(CO_2^-)$ component bands were resolved at 1575 and 1622 cm^{-1}, and they were taken to indicate the coexistence of chelating and bridging coordinations.[24] As shown in Figure 1, the 1548 cm^{-1} band appears at lower Li−methacrylate contents in comparison to the one at 1660 cm^{-1}. This result suggests that at low ionic contents the carboxylate anions in the PMAA phase rearrange to accommodate Li^+ ions in chelating type coordination, while the bridging complexation prevails at higher Li−methacrylate contents and leads to formation of larger anion/cation moieties in the ionic domains.

Complementary information on the interactions between metal ions and their anionic sites in ionic organic and inorganic matrices can be obtained from the far-infrared region where metal ion-site vibrational modes are active.[25–28] Figure 2 depicts the far-infrared spectrum of the SMAA2 diblock copolymer acid and those of the polyelectrolytes synthesized in this work. The acid form exhibits bands at 275, 360, 405, 540, 615, and ca. 650 cm^{-1} (Figure 2a). The strong band at 540 cm^{-1} and the weak feature 405 cm^{-1} are associated with the polystyrene block arising from out-of-plane deformation modes of the benzene ring.[19a,29] Absorption bands in the 200−400 cm^{-1} range (i.e., at 275, 360 cm^{-1}) may be attributed to overlapping contributions of C−C−C bend modes along the polymer backbone in the PS[19] and the PMAA[30] block. The two higher-frequency components at 615 and ca. 650 cm^{-1} are related directly to the anionic site of the diblock copolymers and in particular to the out-of-plane bending and symmetric deformation modes, respectively, of the carboxylic group.[22]

Coordination of Li^+ with carboxylate anions in the PMAA phase leads to the development of a new feature at ca. 420 cm^{-1} (Figure 2b−d), which overlaps with bands already present in the spectra of the acidic forms. On the basis of previous far-infrared studies of alkali metal ionomers[25,26] and glassy lithium acetate,[27] we attribute the 420 cm^{-1} band to Li−O stretching vibration, ν(Li−O), in carboxylate sites. As a result of Li ion−carboxylate interactions, the band appearing at 615 cm^{-1} in the acidic form becomes broader and shifts slightly to higher frequencies (623 cm^{-1}) in the spectra of polyelectrolytes. The spectrum of the polyelectrolyte with the higher Li ion−methacrylate content shows an additional broad band at ca. 195 cm^{-1} and reduced relative intensity at ca. 420 cm^{-1} (Figure 2d). The new feature at ca. 195 cm^{-1} could designate Li−O(site) interactions in aggregates involving a number of Li^+ cations and carboxylate sites close together,[26] which develop at the expense of Li−carboxylate sites giving rise to the primary cation-site vibration band at 420 cm^{-1}. Such band evolution in the far-infrared is consistent with the composition dependence of the 1548 and 1660 cm^{-1} carboxylate bands, as discussed above.

3.2. Thermal Properties and Morphology. Glass transition temperature, T_g, and Δc_p values obtained from thermal analysis of the block copolymers and polyelectrolytes are given in Table 2. It is noted that a single "low" glass temperature was observed in the range 354−373 K, for all samples studied in this work, and corresponds to the PS block.[14] The T_g value of the PMAA block is in the range of ∼500 K,[14] and therefore, the corresponding glass temperature in the copolymers is at higher temperatures than the investigated T range. Nevertheless, the development of Li−O(site) interactions in the PMAA phase, as the IR spectra indicate, is expected to lead to the formation of ionic entities that serve as transient physical cross-links and reduce the mobility of the PMAA chains, resulting in an increase of T_g of the PMAA phase. Generally speaking, the observation of two T_gs in copolymers, per se, cannot suggest the phase state, since even thermodynamically miscible systems exhibit two T_gs.[31] However; the relative insensitivity of the measured low-T_g to copolymer composition (Table 2) is suggestive of phase separation in the PS−PMAA systems. In order to explore the exact phase state, we employ below scattering techniques at the relevant length scale (SAXS).

SAXS measurements can provide information on the effect of Li^+ ions on the block polyelectrolyte microdomain morphology and periodicity. Figure 3 shows representative scattering curves for the block copolymer acids and their Li^+ ion polyelectrolytes at 433 K. Starting from the more asymmetric diblock (SMAA1, $f_{PMAA} = 0.13$), the scattering pattern (Figure 3a) consists of a maximum at a wave vector of 0.25 nm^{-1}, a shoulder with an approximate position $1:3^{1/2}$ relative to the main peak, and a much broader peak at higher wave vectors. Assuming spheres in a bcc lattice, the higher order peaks should appear at relative positions $1:2^{1/2}:3^{1/2}:4^{1/2}:5^{1/2}$. The absence of this sequence of reflections suggests a spherical structure in the absence of long-range order. The broad peak at the higher wave vectors also suggests scattering from a spherical form factor[32] (assigning the intensity minimum at $q = 0.73$ nm^{-1} to the first minimum of the form factor at $qR = 4.484$, results in a sphere radius of 6.1 nm). Complexation of PMAA with Li^+ ions in SMAA1Li has two effects in the SAXS pattern: first, the main peak at q^* shifts to lower q values, and second, higher order peaks appear at relative positions $1:3^{1/2}:7^{1/2}:9^{1/2}$. The former effect shows chain stretching, whereas the latter suggests hexagonally packed cylinders with long-range order. Thus, the effect of complexation with Li^+ is to stiffen the PMAA backbone and to induce a change in the microdomain structure toward more segregated domains (increase in χN, where χ is the interaction parameter and N is the total degree of polymerization, due to increase in χ).[7]

For SMAA2, complexation with Li^+ leads to more drastic effects (Figure 3b). The SMAA2 curve exhibits a broad maximum without higher order peaks, which is characteristic of a disordered block copolymer (correlation hole scattering[7]). However, complexation with Li^+ gives rise to a sharp low q peak and to higher order peaks at relative positions 1:2:3:4:5:

Table 2. Type of Nanostructures and Characteristic Spacings in Diblock Copolymers and in Block Polyelectrolytes Resulting from SAXS Spectra and T_g Temperatures and Δc_p Values Corresponding to PS Resulting from Thermal Analysis

sample	f_{PMAA}, f_{PMAALi}	structure	d_{SAXS}[a] (nm)T = 433 K	$d_{PMAA,Li}$, $R_{PMAA,Li}$ (nm)T = 433 K	T_g^{PS} (K)	Δc_p (J/g K)
SMAA1	0.13	cubic	30.5	8.8/6.1[b]	373	0.30
SMAA1Li	0.14	hex	31.7	6.3	366	0.39
SMAA2	0.23	dis	27.3	6.3	357	0.25
SMAA2Li	0.25	lam	35.3	8.8	362	0.25
SMAA3	0.35	dis			361	0.20
SMAA3Li	0.37	dis			354	0.24

[a] The spacings for lamellar, cubic, and hexagonally packed patterns were determined respectively as $d = 2\pi/q^*$, $d = (2\pi/q^*)(3/2)^{1/2}$ and $d = (2\pi/q^*)(4/3)^{1/2}$, in which q^* is the position of the first peak in SAXS plots. The size of the minority phase can be calculated from Bragg spacings and geometrical considerations as $d_{PMAALi} = f_{PMAALi}d$, for the lamellar forming copolymer, as $R_{PMAA} = (f_{PMAA}d^3/3^{1/2}\pi)^{1/3}$, for the bcc lattice, and as $R_{PMAALi} = (3^{1/2}f_{PMAALi}d^2/2\pi)^{1/2}$, for the hexagonal packing of cylinders. [b] Estimated from the form factor minimum.

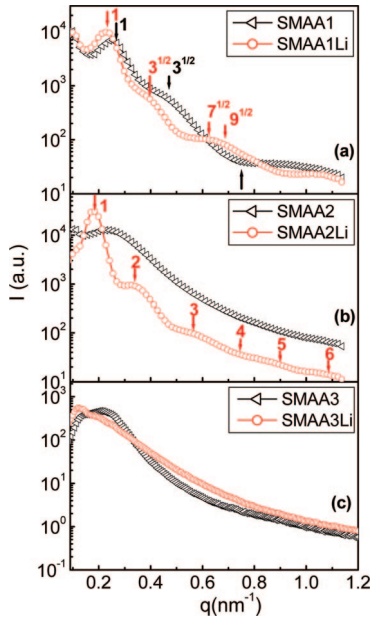

Figure 3. SAXS curves from the diblock copolymers and the resulting block polyelectrolytes. (a) SMAA1 (f_{PMAA} = 0.13, T = 433 K): arrow indicates peak at positions $1:3^{1/2}$ relative to the main peak; SMAA1Li (f_{PMAALi} = 0.14, T = 433 K): arrows indicate peaks at positions $1:3^{1/2}:7^{1/2}:9^{1/2}$ relative to the main peak (the up arrow in the figure gives the form factor minimum). (b) SMAA2 (f_{PMAA} = 0.23, T = 433 K): in disordered phase; SMAA2Li (f_{PMAALi} = 0.25, T = 433 K): arrows indicate peaks at positions 1:2:3:4:5:6 relative to the main peak. (c) SMAA3 (f_{PMAALi} = 0.35, T = 363 K): in the disordered phase, SMAA3Li (f_{PMAALi} = 0.37, T = 363 K): in the disordered phase.

6. These reflections clearly show the formation of a lamellar microdomain morphology with long-range order. Thus, the effect of complexation here is to drive the system from the disordered phase directly to the lamellar morphology. Again, this is not the result of the (slight) change in the volume fraction but is solely due to the increase in χ.

Contrary to SMAA1 and SMAA2, complexation of SMAA3 with Li^+ ions does not change appreciably the microdomain morphology (Figure 3c). Both acid and block polyelectrolyte curves exhibit a broad maximum that reveals a disordered phase (the feature at low wavevectors reflects parasitic scattering). Nevertheless, this broad peak is shifted to lower q upon complexation. Thus, chain stretching is observed in all block polyelectrolytes, and this results in a change of the microdomain morphology provided that N is high enough (SMAA1 and SMAA2). Alternatively, the absence of ordering in SMAA3Li could result from the high ionic content and the higher degree of ionic cross-linking of the PMAA chains in the particular material (see Table 1 and the results from IR spectroscopy), which do not allow for adequate relaxation of the PMAA block even at the highest temperature investigated. The results on the morphology and domain spacings from SAXS are summarized in Table 2.

The present results on the microdomain morphology are consistent with the results of an electric field study on PS-*b*-PMMA/LiCl by Wang et al.[33,34] It was shown that lithium−PMMA complexation produces a significant increase of the dielectric constant, and this effectively reduces the critical electric field strength necessary to overcome the preferrential interaction of one block with the substrate. Such an effect gave rise to a complete microdomain alignment. In addition, a study on the influence of ionic complexes on the phase behavior of PS-*b*-PMMA by Wang et al.[35] showed that the formation of lithium−PMMA complexes increases the overall Flory−Huggins segmental interaction parameter, χ_{eff} (between the PS block and the PMMA complexed phase), relative to χ_{eff} of parent copolymes. This effect led to the increase in ordering and spacing of the microdomains.

3.3. Dynamics. DS can be employed as a sensitive tool of the local dynamics in copolymers[36–39] and polymer−salt complexes[40–42] over broad temperature and frequency ranges. Investigating the ion dynamics in the present case is of particular importance since the IR investigation has shown that Li^+ ions are confined within the PMAA domain through complexation. It is therefore natural to ask how this complexation affects the local ion mobility as well as the dc conductivity. More specifically, we are interested in how the chelating and bridging Li^+ ion coordination affects the local ion dynamics and the more global dc conduction. We mention here parenthetically that a recent study[43] revealed enhanced ion mobility in polymer/clay nanocomposites.

Figure 4 presents superpositions of the real and imaginary parts of the dielectric permittivity ε^*, the electric modulus M^*, and the conductivity σ^* for the diblock copolymer SMAA1 at a reference temperature of 433 K. The three representations of the dielectric data are complementary and emphasize different aspects of the same processes. The superpositions were made around the M'' maximum, and the same horizontal shift factors, a_T, were used for the ε^* and σ^* representations. Note that in all representations the crossing of the real and imaginary parts occurs at the same frequency, which signifies the process due to ion relaxation. The electric modulus representation reveals a main contribution at lower frequencies ($\sim 10^{-2}$ Hz) due to ion mobility and an additional weak process (called α-process) at higher frequencies ($\sim$1 Hz). The dielectric permittivity representation provides evidence for the α-process, while the conductivity representation emphasizes the dc and ac charge carrier mobility at low and high frequencies, respectively. The extracted relaxation times, $\tau_{M''_{max}}$, from frequencies corresponding to M''_{max} for the weak α-process in all block copolymers are found to follow the Vogel−Fulcher−Tammann (VFT) equation:

$$\tau_{max} = \tau_0 \exp\left(\frac{D_T T_0}{T - T_0}\right) \quad (6)$$

where τ_0 is the relaxation time in the limit of very high temperatures ($=10^{-14}$ s), B ($=D_T T_0$) is the apparent activation

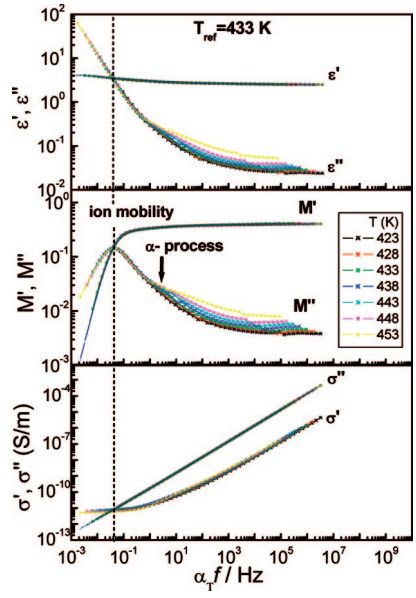

Figure 4. Superpositions of the real and imaginary parts of the complex dielectric permittivity, ε^*, the electric modulus, M^*, and the conductivity, σ^*, for the diblock copolymer SMAA1 at a reference temperature of 433 K. The superimposed data sets are taken in 5 K increments within the temperature range 423−453 K. The dashed lines give the process due to ion mobility.

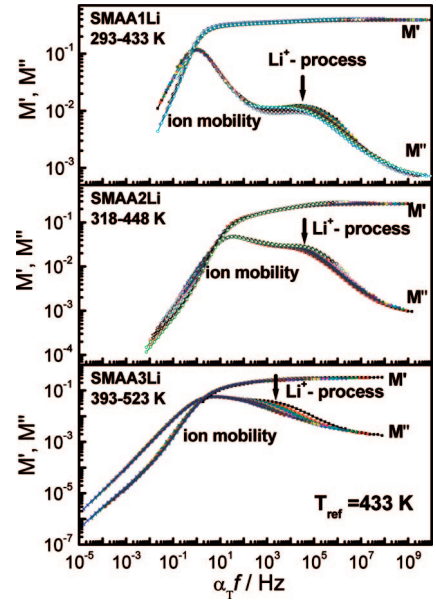

Figure 5. Superpositions of the real and imaginary parts of the complex electric modulus, M^*, for the three block polyelectrolytes: (top) SMAA1Li, (middle) SMAA2Li, and (bottom) SMAA3Li, at a reference temperature of 433 K. The superimposed data sets are taken in 5 K increments within the temperature ranges 293−433 K (SMAA1Li), 318−448 K (SMAA2Li), and 393−523 K (SMAA3Li). The two M'' maxima at lower and higher frequencies reflect the ion mobility and lithium ion processes, respectively.

parameter, D_T is a dimensionless parameter (=14.4 for SMAA1), and T_0 is the "ideal" glass temperature (294 K for SMAA1). This process corresponds to the segmental dynamics within the PS domains. The glass transition temperature, defined in DS as the temperature with a corresponding α-relaxation time of $\tau \sim 10^2$ s, is at ~400 K for SMAA1. This value is higher than the DSC T_g (Table 2) probably because of the small frequency range that this mode is probed. Since this process is relatively weak, in the block polyelectrolytes it is completely masked by stronger processes related to the Li^+ ion dynamics and, therefore, will not be discussed further.

Figure 5 gives the electric modulus representation for the corresponding block electrolytes. The benefit from such representations is that all processes appear within the scaled frequency window, and thus, deviations from the time−temperature superposition can be easily detected. For example, both the crossing of the real and imaginary parts at low frequencies (resulting from the ion mobility) as well as faster processes associated here with the Li ion process can be obtained from a single curve. A comparison of the ion mobility process for the SMAA1 and SMAA1Li copolymers (Figures 4 and 5) reveals an acceleration in the case of the block electrolyte under isochronal conditions ($T_{ref} = 433$ K). For example, the crossing of M' and M'' occurs at $\sim 4 \times 10^{-2}$ Hz for SMAA1, while for SMAA1Li it moves to $\sim 7 \times 10^{-1}$ Hz. In addition, the value of the dc ionic conductivity for SMAA1 is $\sigma_{dc} \approx 10^{-12}$ S m^{-1} at 433 K, indicating an insulator, while introduction of Li^+ ions in the methacrylic phase increases the conductivity by 2 orders of magnitude. The T dependence of the dc conductivity, obtained from the low-frequency plateau of σ', is depicted in Figure 6 for the SMAA1Li block polyelectrolyte and compared to the corresponding SMAA1 diblock. The dc conductivity exhibits a typical Arrhenius temperature dependence

$$\sigma_{dc} = \sigma_0 \exp\left(-\frac{E}{RT}\right) \tag{7}$$

where σ_0 is the conductivity in the limit of infinite temperature and E is the apparent activation energy, with values of 185 and 69 kJ/mol for SMAA1 and SMAA1Li, respectively. A similar

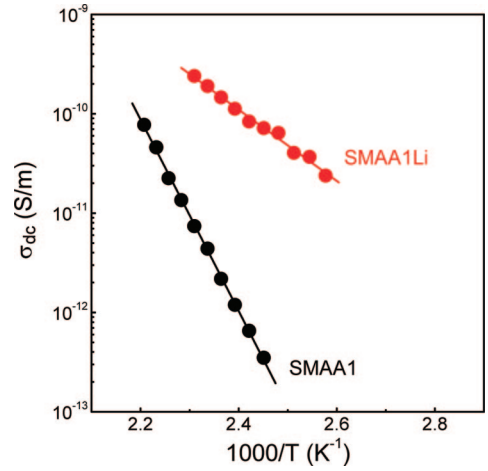

Figure 6. Temperature dependence of dc conductivity for the SMAA1 block copolymer and the corresponding block polyelectrolyte (SMAA1Li). The lines represent fits to an Arrhenius law.

Table 3. Activation Energies for dc Conductivity (E) of Diblock Copolymers and of the Resulting Block Polyelectrolytes and Parameters (τ_0, E^*) of the Arrhenius Equation for the Local Li^+ Ion Relaxation Mechanism in Block Polyelectrolytes

sample	E (kJ/mol)	$-\log(\tau_0/s)$	E^* (kJ/mol)
SMAA1	185 ± 2		
SMAA1Li	69 ± 2	−14	81 ± 2
SMAA2	230 ± 5		
SMAA2Li	66 ± 3	−14	87 ± 2
SMAA3	145 ± 2		
SMAA3Li	130 ± 2	−16	117 ± 3

decrease of E was observed for the SMAA2 case, whereas for SMAA3 and SMAA3Li the activation energies were 145 and 130 kJ/mol, respectively (Table 3). Thus, introduction of Li^+ ions in SMAA1 and SMAA2 effectively softens the potential and increases the conductivity.

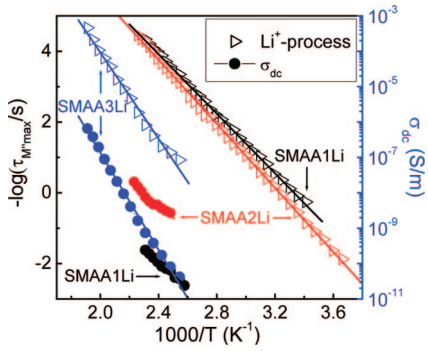

Figure 7. Relaxation map of the parameters of the Arrhenius equation for the local Li^+ ion relaxation mechanism (open symbols, left axis) and dc conductivity (filled symbols, right axis) for the block polyelectrolytes: SMAA1Li (black), SMAA2Li (red), and SMAA3Li (blue). The lines are fits to an Arrhenius equation.

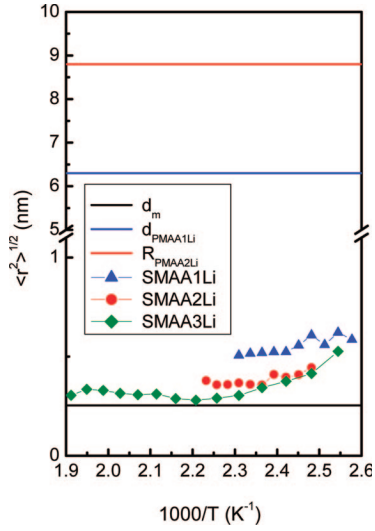

Figure 8. Mean-square displacement for block polyelectrolytes SMAA1Li (triangles), SMAA2Li (circles), and SMAA3Li (rhombus) in comparison to the length of a monomer unit (black line) and domain spacing for SMAA1Li (blue line) and SMAA2Li (red line).

Following the introduction of Li^+ ions, a new dynamic process appears in the electric modulus representation (Figure 5) indicated by the second M'' maximum at higher frequencies. It is noted that the shifted electric moduli data at the different temperatures investigated do not conform to a single master curve, suggesting that the new process has a slightly different T dependence from the process associated with the ionic mobility, and this is more evident for SMAA3Li. This process is characterized by peak shape parameters $m = mn = 0.42$ and a weak T dependence that conforms to an Arrhenius dependence

$$\tau_{max} = \tau_0 \exp\left(\frac{E^*}{RT}\right) \tag{8}$$

with activation parameters that are also summarized in Table 3. Slower relaxation processes than the polymer segmental relaxation have been observed in ionomer and polymer−salt systems[40–42] and have been attributed to cation fluctuations in temporar confinements of the ionic domain (acting as temporar cross-links). However, this new process here appears within the PMAA phase, and thus, it reflects a low-amplitude localized PMAA/Li cooperative process. The T dependence of the relaxation times associated with the new Li^+ ion process and of the process due to ion conductivity are compared for the three block polyelectrolytes in Figure 7. This figure reveals almost identical relaxation times for the local Li^+ ion process in SMAA1Li and SMAA2Li and slower dynamics in SMAA3Li. This finding reflects likely difference in coordination of Li^+ ion in polyelectrolytes with low and high ionic contents, respectively. The identical dynamics of Li^+ ions in SMAA1Li and SMAA2Li reflect localized Li^+ ion dynamics in chelating coordination. The slower dynamics in SMAA3Li reflect the higher restrictions imposed to Li^+ ions by the bridging coordination. In the latter, the presence of larger anion/cation moieties in the ionic domains produce stronger correlations that are reflected on the much slower local ion dynamics. Nevertheless, this local process does not contribute to the dc conductivity. In addition to these processes, one can notice the nearly parallel M' and M'' dependencies in the low-frequency side (Figure 5). The process known as the Maxwell−Wagner−Sillars polarization, due to blocking of charge carriers at the interfaces, influences the dielectric response of heterogeneous systems at low frequencies/high temperatures. However, the analysis of this mechanism requires even higher temperatures/lower frequencies, the former being precluded by sample decomposition.

Returning to the process responsible for the ionic conduction, we explore the characteristic step length for the ion motion in relation to the PMAA nanodomain size. On the basis of hydrodynamics, one can relate the dc conduction to the diffusion coefficient, D_i, of ionic traces through the Nernst−Einstein relations as

$$D_i = \frac{\sigma_{dc} k_B T}{Ne^2} \tag{9}$$

where N is the number of ions each of charge e. The microscopic ion motion can be modeled as a random walk with step length, $\langle r^2\rangle^{1/2}$, and step time, τ, through the Einstein−Smoluchowski equation.

$$D_i = \frac{\langle r^2\rangle}{6\tau} \tag{10}$$

From eqs 9 and 10, we obtain the relation between the dc conductivity and the step length as

$$\sigma_{dc} = \frac{Ne^2}{6k_B T}\frac{\langle r^2\rangle}{\tau} \tag{11}$$

In the present case of microphase-separated block copolymers, the ions are confined within the PMAA domains with dimensions of 6.3 and 8.8 nm, in the case of SMAA1Li ($f_{PMAALi} = 0.14$, hexagonally packed cylinders) and SMAA2Li ($f_{PMAALi} = 0.25$, lamellae) block polyelectrolytes, respectively, that give the upper limit to the ion displacement. Approximating the step time with $\tau_{M''_{max}}$, i.e., with the characteristic time of ionic motion, and employing the measured σ_{dc} (Figures 4 and 6) results in a mean-square displacement of ∼0.7 and 0.5 nm for SMAA1Li and SMAA2Li, respectively (Figure 8). The smaller values of the characteristic step length, as compared to the domain spacing, suggest that several events are needed for the Li^+ ions to explore the anionic domain. Furthermore, $\langle r^2\rangle^{1/2}$ is of the order of the monomer size (∼0.25 nm), suggesting that ions hop from one methacrylic segment to another during the $\tau_{M''_{max}}$ time scale. Thus, the fundamental contribution to macroscopic ionic conduction is intersegmental ion hopping, and it takes several events for an ion to explore the whole anionic domain. We mention here, parenthetically, that a recent study[44] on the origin of the liquid-to-glass formation in glass-forming systems identified the monomer unit as the basic structural unit related to the dynamic arrest at the glass transition.

4. Conclusions

The local structure, microdomain morphology, and ion dynamics of block copolymers of PS−PMAA and of their

corresponding Li−block polyelectrolytes were investigated by infrared spectroscopy (IR), small-angle X-ray scattering (SAXS), differential scanning calorimetry (DSC), and dielectric spectroscopy (DS). Mid-infrared spectroscopy revealed the mode of complexation of Li^+ ions with carboxylate units of the PMAA phase, i.e., chelating type coordination and bridging type complexation in larger ionic entities as the Li−PMAA content increases. Complementary information was obtained by far-infrared spectroscopy which revealed the presence of Li^+ ion-site vibration bands related to ionic segments involving few ions at low Li−PMAA contents and to aggregates of many ions at higher Li−PMAA contents. The stronger segregation resulting from the introduction of Li^+ ions in the PMAA phase alters the phase state and induces a cubic-to-cylinder transformation in SMAA1 and a disorder-to-lamellar transformation in SMAA2. However, the SMAA3/SMAA3Li systems are characterized by disorder, probably due to extensive ionic aggregation effects. In addition, Li^+ ion-induced chain stretching was observed in all cases, consistent with a change from the weak- to strong-segregation limit. Investigation of dynamics revealed a new dielectrically active process associated with a local relaxation of Li^+ ions coupled to the MAA segments. The progressive change of Li^+ ion coordination in the PMAA phase of block polyelectrolytes upon increasing the PMAA content was found to slow down the Li^+ ion dynamics by about 2 orders of magnitude. The ionic conductivity of the block polyelectrolytes increased by about 3 orders of magnitude relative to the corresponding acidic form. Ion motion is bound to PMAA segments, and several intersegmental Li^+ ion hopping events in the channels of the PMAA phase are necessary to explore the whole ionic domain.

Acknowledgment. Partial support of this work through the "Excellence in the Research Institutes" program, supervised by the General Secretariat for Research and Technology/Ministry of Development, Greece (Phase I and II, Projects 64769 and 2005ΣΕ01330081), is gratefully acknowledged. Support by the GSRT in the framework of PENED03 (03ED856) is also gratefully acknowledged.

References and Notes

(1) Chandrasekhar, V. *Adv. Polym. Sci.* **1998**, *135*, 139–205.
(2) Tarascon, J. M.; Armand, M. *Nature (London)* **2001**, *414*, 359–367.
(3) Wright, P. V. *MRS Bull.* **2002**, *27*, 597–601.
(4) Ryu, S.; Trapa, P.; Olugebefola, S.; Gonzalez-Leon, J.; Sadoway, D. R.; Mayes, A. M. *J. Electrochem. Soc.* **2005**, *152*, A158–A163.
(5) Soo, P. P.; Huang, Y. I.; Olugebefola, S.; Chiang, Y. M.; Sadoway, D. R.; Mayes, A. M. *J. Electrochem. Soc.* **1999**, *146*, 32–37.
(6) Watanabe, M.; Oohashi, S. I.; Sanui, K.; Ogata, N.; Kbayashi, T.; Ohtaki, Z. *Macromolecules* **1985**, *18*, 1945–1950.
(7) (a) Hamley, I. A. In *The Physics of Block Copolymers*; Oxford University Press: Oxford, 1998. (b) Hadjichristidis, N.; Pispas, S.; Floudas, G. In *Block Copolymers: Synthetic Strategies, Physical Properties and Applications*; Wiley-Interscience: New York, 2002.
(8) Trapa, P.; Huang, B.; Won, Y.-Y.; Sadoway, D. R.; Mayes, A. M. *Electrochem. Solid-State Lett.* **2002**, *5*, A85–A88.
(9) Konradi, R.; Rühe, M. *Macromolecules* **2004**, *37*, 6954–6961.
(10) Walters, R. M.; Sohn, K. E.; Winey, K. I.; Composto, R. J. *J. Polym. Sci., Part B: Polym. Phys.* **2002**, *41*, 2833–2841.
(11) Benetatos, N. M.; Winey, K. I. *Macromolecules* **2007**, *40*, 3223–3228.
(12) (a) Hadjichristidis, N.; Iatrou, H.; Pispas, S.; Pitsikalis, M. *J. Polym. Sci., Part A: Polym. Chem.* **2000**, *38*, 3211–3234. (b) Uhrig, D.; Mays, J. W. *J. Polym. Sci., Part A: Polym. Chem.* **2005**, *43*, 6179–6222.
(13) (a) Pispas, S.; Siakali-Kioulafa, E.; Hadjichristidis, N.; Mavromoustakos, T. *Macromol. Chem. Phys.* **2002**, *203*, 1317–1327. (b) Pispas, S.; Hadjichristidis, N. *Macromolecules* **2003**, *36*, 8732–8737. (c) Pispas, S. *J. Phys. Chem. B* **2006**, *110*, 2649–2655.
(14) Brandrup, J.; Immergut, E. H.; Grulke, E. A. In *Polymer Handbook*; John Wiley and Sons: New York, **1999**.
(15) Floudas, G. In *Broadband Dielectric Spectroscopy*; Kremer, F., Schönhals, A., Eds.; Springer: New York, 2002; Chapter 8.
(16) Havriliak, S.; Negami, S. *Polymer* **1967**, *8*, 161–210.
(17) McCrum, N. G.; Read, B. E.; Williams, G. In *Anelastic and Dielectric Effects in Polymeric Solids*; Dover: New York, 1991.
(18) Richert, R.; Wagner, H. *Solid State Ionics* **1998**, *105*, 167–173.
(19) (a) Liang, C. Y.; Krimm, S. *J. Polym. Sci.* **1958**, *XXVII*, 241–254. (b) Versanyi, G. In *Vibrational Spectra of Benzene Derivatives*; Academic Press: New York, 1969; p 302.
(20) Hesse, M.; Meier, H.; Zeeh, B. In *Spectroscopic Methods in Organic Chemistry*; Enders, D., Noyori, R., Trost, B. M., Eds.; Organic Chemistry Series; Thieme: New York, 1997; Vol. *2*, pp 44, 55.
(21) Grigor'ev, A. I. *Russ. Inorg. Chem.* **1963**, *8*, 409–414.
(22) Donaldson, J. D.; Knifton, J. F.; Ross, S. D. *Spectrochim. Acta* **1965**, *21*, 275–277.
(23) Painter, P. C.; Brozoski, B. A.; Coleman, M. *J. Polym. Sci., Polym. Phys. Ed.* **1982**, *20*, 1069–1080.
(24) Barreto, L. S.; Mort, K. A.; Jackson, R. A.; Alves, O. L. *J. Non-Cryst. Solids* **2002**, *303*, 281–290.
(25) Tsatsas, A. T.; Reed, J. W.; Risen, W. M., Jr *J. Chem. Phys.* **1971**, *55*, 3260–3269.
(26) Rouse, G. B.; Risen, W. M., Jr.; Tsatsas, A. T.; Eisenberg, A. *J. Polym. Sci., Polym. Phys. Ed.* **1979**, *17*, 81–85.
(27) Kamitsos, E. I.; Chryssikos, G. D. *Solid State Ionics* **1998**, *105*, 75–85.
(28) Gatsouli, K. D.; Pispas, S.; Kamitsos, E. I. *J. Phys. Chem. C* **2007**, *111*, 15201–15209.
(29) (a) Jasse, B.; Monnerie, L. J. J. *Mol. Struct.* **1977**, *39*, 165. (b) Rabolt, J. F.; English, A. D. *Macromolecules* **1989**, *22*, 2867–2869.
(30) Snyder, R. G.; Schachtschneider, J. H. *Spectrochim. Acta* **1962**, *19*, 85–116.
(31) (a) Lodge, T. P.; McLeish, T. C. B. *Macromolecules* **2000**, *33*, 5278–5284. (b) Lodge, T. P.; Wood, E. R.; Haley, J. C. *J. Polym. Sci., Polym. Phys. Ed.* **2006**, *44*, 756–763.
(32) (a) Kinning, D. J.; Thomas, E. L. *Macromolecules* **1984**, *17*, 1712–1718. (b) Bourlinos, A. B.; Giannelis, E. P.; Zhang, Q.; Archer, L. A.; Floudas, G.; Fytas, G. *Eur. Phys. J. E* **2006**, *20*, 109–117.
(33) Wang, J.-Y.; Ting, X.; Leiston-Belanger, J. M.; Gupta, S.; Russell, T. P. *Phys. Rev. Lett.* **2006**, *96*, 128301-1–128301-4.
(34) Wang, J.-Y.; Leiston-Belanger, J. M.; Sievert, J. D.; Russell, T. P. *Macromolecules* **2006**, *39*, 8487–8491.
(35) Wang, J.-Y.; Chen, W.; Roy, C.; Sievert, J. D.; Russell, T. P. *Macromolecules* **2008**, *41*, 963–969.
(36) Floudas, G.; Hadjichristidis, N.; Iatrou, H.; Pakula, T. *Macromolecules* **1996**, *29*, 3139–3146.
(37) Floudas, G.; Fytas, G.; Pispas, S.; Hadjichristidis, N.; Pakula, T.; Khokhlov, A. R. *Macromolecules* **1995**, *28*, 5109–5118.
(38) Floudas, G.; Fytas, G.; Reisiner, T.; Wegner, G. *J. Chem. Phys.* **1999**, *111*, 9129–9132.
(39) Floudas, G.; Paraskeva, S.; Hadjichristidis, N.; Fytas, G.; Chu, B.; Semenov, A. N. *J. Chem. Phys.* **1997**, *107*, 5502–5509.
(40) Furukawa Mukasa, Y.; Suzuki, T.; Kano, K. *J. Polym. Sci., Polym. Phys. Ed.* **2002**, *40*, 613–622.
(41) Zhang, S.; Runt, J. *J. Phys. Chem. B* **2004**, *108*, 6295–6302.
(42) Atorngitjawat, P.; Runt, J. *J. Phys. Chem. B* **2007**, *111*, 13483–13490.
(43) Elmahdy, M. M.; Chrissopoulou, K.; Afratis, A.; Floudas, G.; Anastasiadis, S. H. *Macromolecules* **2006**, *39*, 5170–5173.
(44) Floudas, G.; Mpoukouvalas, K.; Papadopoulos, P. *J. Chem. Phys.* **2006**, *124*, 074905-1–074905-5.

MA8008542